ANNALS OF GEOPHYSICS, 65, 4, SE425, 2022; doi:10.4401/ag-8636
OPEN ACCESS

Semi-automated stochastic simultaneous simulation of macroseismic information and strong ground motion records for recent strong earthquakes of the Aegean area

Michail Ravnalis[*,1], Charalampos Kkallas[1], Constantinos Papazachos[1], Basil Margaris[2] and Christos Papaioannou[2]

(1) Department of Geophysics, Aristotle University of Thessaloniki, Greece
(2) Institute of Earthquake Engineering and Engineering Seismology, Kalamaria, Greece

Article history: received February 4, 2021; accepted March 29, 2022

Abstract

We apply a stochastic simulation approach for the simultaneous modeling of macroseismic data and strong ground motion records for several shallow strong earthquakes ($M \geq 6.0$) that occurred in the Aegean area from 1980 to 1995 Alkyonides (1981, **M**6.7), Kalamata (1986, **M**6.0), Kozani (1995, **M**6.6) and Aigio (1995, **M**6.4). The application is semi-automatic, as several of the selected input parameters for the stochastic simulation modeling were automatically calibrated using a priori information (e.g., magnitude, stress parameter, site effects). Other parameters (e.g., fault type, depth) were pre-determined, based on published information, most of which are usually derived during standard earthquake analysis. The validity and reliability of this approach was examined, to test if this method could be applied either in a fully automated manner, or for the study of source properties of historical earthquakes. While the results obtained from the semi-automated simulations were satisfactory, they also suggest that it is not possible to achieve the same level of reliability and robustness when modeling complicated seismic sequences, as e.g., is the case of the Alkyonides earthquake (1981, **M**6.7).

Keywords: Seismology; Stochastic simulation; Macroseismic observations; EXSIM; Aegean area; Strong ground motion

1. Introduction

The Aegean region is one of the most tectonically active areas of the Mediterranean, exhibiting high shallow and intermediate depth seismicity, including large subduction (up to **M**~8.0) and back-arc (up to ~**M**7.5) earthquakes [Papazachos, 1990]. For the study of historical earthquakes only the available macroseismic observations are used in practice, as instrumental data do not exist for these events. The geographical distribution of macroseismic intensities provides valuable information on the seismic source, path attenuation and site amplification

effects, while the largest macroseismic intensities usually cluster and often delineate the near-fault source region [Papazachos and Papazachou, 1997]. On the other hand, the increasing availability of strong motion accelerograms makes the use of seismic records an even more attractive option for defining information useful for the study of the source-path-site triplet factor. While peak ground motion values (PGA, PGV and PGD) are often used to quantify strong ground motion, as they show a strong correlation with damage [e.g., Kramer, 1996], response and Fourier spectra are also extracted from instrumental records, as they provide valuable information on the frequency content of strong ground motions.

Usually, macroseismic and strong motion information have been used independently (in Greece, but also worldwide) for the study of strong earthquakes. Figure 1 depicts the smoothed annual collection rates of strong ground motion data (blue line) and macroseismic observations with Modified Mercalli intensity values (I_{MM}) larger or equal to 5, respectively, for Greece (Database of Geophysical Laboratory, Aristotle University of Thessaloniki; HEAD database [http://www.itsak.gr/head/]; Theodulidis et al., [2004]. Starting from roughly 1980, an exponential increase of instrumental data is observed, while from 1995 onwards there is a gradual decrease of the macroseismic data collection rate. Due to the above, we selected strong earthquakes ($\mathbf{M} \geq 6.0$) that occurred during 1978-1995, for which an adequate number of both macroseismic intensities and instrumental recordings was available (orange area in Figure 1). During this period, not only a large number of macroseismic observations is still available for most strong mainshocks, but also a gradual increase of the available strong ground motion records (accelerograms) is observed.

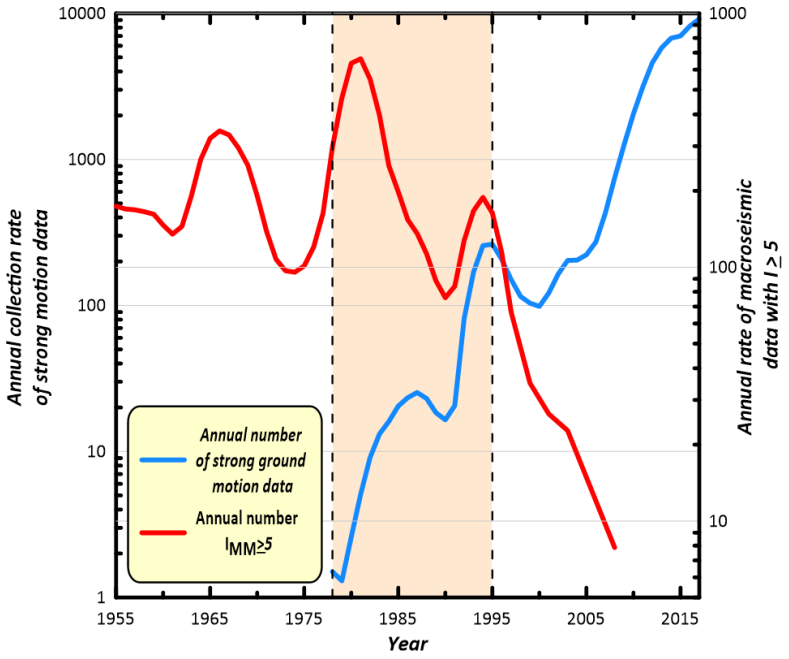

Figure 1. Smoothed annual collecting rate of strong ground motion records and macroseismic observations with $I_{MM} > 5$ (blue and red line, respectively). The orange area indicates the time period for which data are used in the present work.

The method of stochastic simulation of strong ground motion is a widely used tool that is employed to generate synthetic data to study the spatial distribution of strong ground motion after a significant earthquake. Starting for the pioneering works of Boore [1983] and Boore and Atkinson [1987] stochastic simulations have been used in several applications for strong ground motion studies. More specifically, the finite fault simulation approach was applied for historical earthquakes in Greece, for which only damage information (macroseismic intensities) was available [Papazachos et al., 2015; Kkallas et al., 2018]. Papazachos et al. [2015] used stochastic simulation to model the spatial distribution of the strong ground motion for the large historical earthquakes of Sofades (1954, **M**7.0) and Velestino (1957, **M**6.8) (southern Thessaly basin, central Greece), using observed macroseismic intensities (I_{MM} up to 9+). Kkallas et al. [2018] modelled the macroseismic damage distribution of several intermediate-depth

earthquakes of the southern Aegean subduction zone. Moreover, stochastic simulation has been employed for the study of several strong earthquakes that occurred in Greece, for which instrumental (mainly strong motion) data were available [e.g., Roumelioti et al., 2000; Benetatos and Kiratzi, 2004; Mavroeidis et al., 2018]. This approach has been widely used for the estimation of the peak parameters of ground motion in several regions worldwide [e.g., Motazedian and Moinfar, 2006; Galluzzo, Zonno, and Del Pezzo, 2008; Zonno et al. 2010; Ghofrani et al., 2013; Dang and Liu, 2020], in an attempt to estimate and reconstruct the main features of strong ground motion for finite-fault mainshocks.

It is evident that while strong historical earthquakes have been almost exclusively studied with the use of their macroseismic data, the contribution of instrumental records (mainly for recent earthquakes) is also critical, as it provides valuable and detailed constraints for the study of various earthquake parameters (source, propagation path, etc.), as well as their impact. The purpose of the present study was to explore the possibility to perform a simultaneous, joint interpretation of these two types of data (macroseismic data and strong motion data) for selected shallow earthquakes in Greece. The study focuses on events which have occurred in the time period 1978-1995, depicted in Figure 1, for which both data types was available. Moreover, we adopt a simulation approach where most input parameters used for the simulation of macroseismic and strong motion data have been determined in a semi-automated manner. The main motivation for this automation was to examine the possibility to either fully automatize the process (for recent data) or to apply it for historical earthquakes, for which detailed seismic source, propagation path and site effect information is usually limited or simply not available.

2. Data

For the period 1978-1995, depicted in Figure 1, we have identified six (6) $\mathbf{M} > 6.0$ mainshock (no aftershocks were considered), for which both macroseismic and strong-motion data were available. In the present study we consider four (4) out of these 6 significant ($\mathbf{M} \geq 6.0$) shallow earthquakes and employed the finite-fault stochastic simulation method to model their damage distribution, as well as the available accelerograms (strong motion records). These four mainshocks are the Alkyonides (1981, **M**6.7), Kalamata (1986, **M**6.0), Kozani (1995, **M**6.6) and Aigio (1995, **M**6.4) earthquakes. Table 1 summarizes the information of every earthquake considered in this paper, using the information provided by Papazachos and Papazachou [1997]. The two $M \geq 6.0$ earthquakes for which we do not present results in this study are the Thessaloniki (1978, **M**6.5) mainshock, for which limited strong motion data from a single city (Thessaloniki) were available, and the Kyllini (1998, **M**6.0) event, which was located at sea and for which we had no constraints on the fault rupture. In Figure 2 the focal mechanisms of the four strong shallow earthquakes which were simulated in this paper are depicted. It should be noticed that all the examined earthquakes were normal faulting events, which is typical for most events of the Greek mainland.

Macroseismic data were collected from the published databank of macroseismic information for the Aegean area [Papazachos et al., 1997]. This databank includes macroseismic observations available for several Greek set-

Earthquake		Origin time (yyyy/mm/dd, hh:mm)	Latitude	Longitude	h (km)	M	ζ (°)	δ (°)	λ (°)
1	Alkyonides	1981/02/24, 20:53	38.20	23.00	10	6.7	264	42	−80
2	Kalamata	1986/09/13, 17:24	37.10	22.20	6	6.0	200	50	−81
3	Kozani	1995/05/13, 08:47	40.20	21.70	14	6.6	240	45	−101
4	Aigio	1995/06/15, 00:15	38.40	22.20	12	6.4	276	33	−76

Table 1. Information on the 4 earthquakes considered in this study [Papazachos and Papazachou, 1997] (**M**: moment magnitude, h: focal depth, ζ: Fault Strike, δ: Fault Dip, λ: Rake).

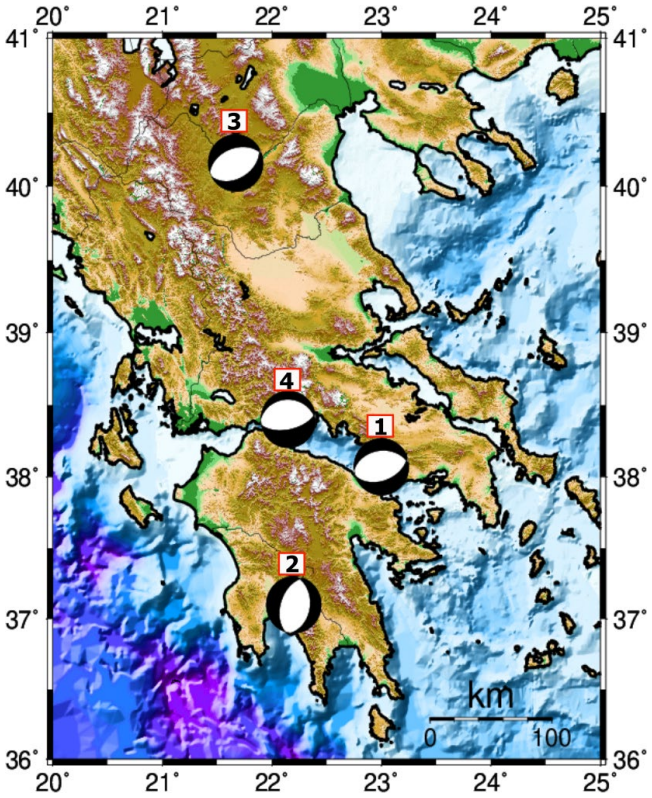

Figure 2. Focal mechanisms of the four earthquakes that were studied in the present work [Alkyonides (1), Kalamata (2), Kozani (3) and Aigio (4) earthquakes].

tlements (Intensity Data Points (IDP) in Modified Mercalli, with intensity values up to 10). As the IDP geographical coordinates were based on old and approximate settlement location information, it was necessary to cross-validate the IDP database coordinates. We used an automated IDP location correction approach, that matched the available settlement names and epicentral distances between the database locations and the updated, high-precision geographical coordinates available for all settlements of Greece from the National Cadaster. An example of the original and relocated IDP locations for the Aigio earthquake (1995, **M**6.4) is presented in Figure 3. The average

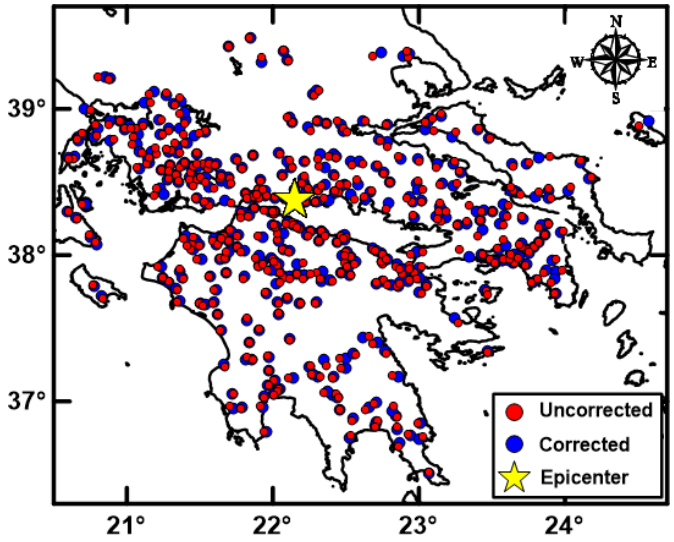

Figure 3. Spatial distribution of the geographically corrected IDP (blue solid circles) in comparison to the original IDP (red solid circles) of the Papazachos et al. [1997] database for the Aigio earthquake (1995, M6.4).

IDP relocation (distance correction) was 1.7 km for the four earthquakes examined, which could be considered as an indicative settlement accuracy of the original Papazachos et al. [1997] macroseismic database. While this error is not negligible, it is not expected have a critical effect on the obtained results, except for IDP in the immediate vicinity of the seismic source.

In the present work we considered all available strong motion data at epicentral distances up to 100 km, since we wanted to capture the near-fault strong motion distribution. The data were collected from the HEAD database (http://www.itsak.gr/head/) and have been processed according to the approach proposed by Trifunac and Todorovska [2001] and Skarlatoudis et al. [2003], which allows for the automatic determination of the filtering parameters (for older, analogue accelerograms), on the basis of the corresponding earthquake magnitude and epicentral distance. For the purposes of the present work, we employed (and fitted) the Fourier Amplitude Spectra (FAS) of the strong motion data for each available station. Due to the previously mentioned filtering, only a part of the FAS is reliable, especially for older analogue recordings that often have a rather narrow useful FAS bandwidth [Skarlatoudis et al., 2003]. A typical example of a recording and its useful FAS segment is presented in Figure 4.

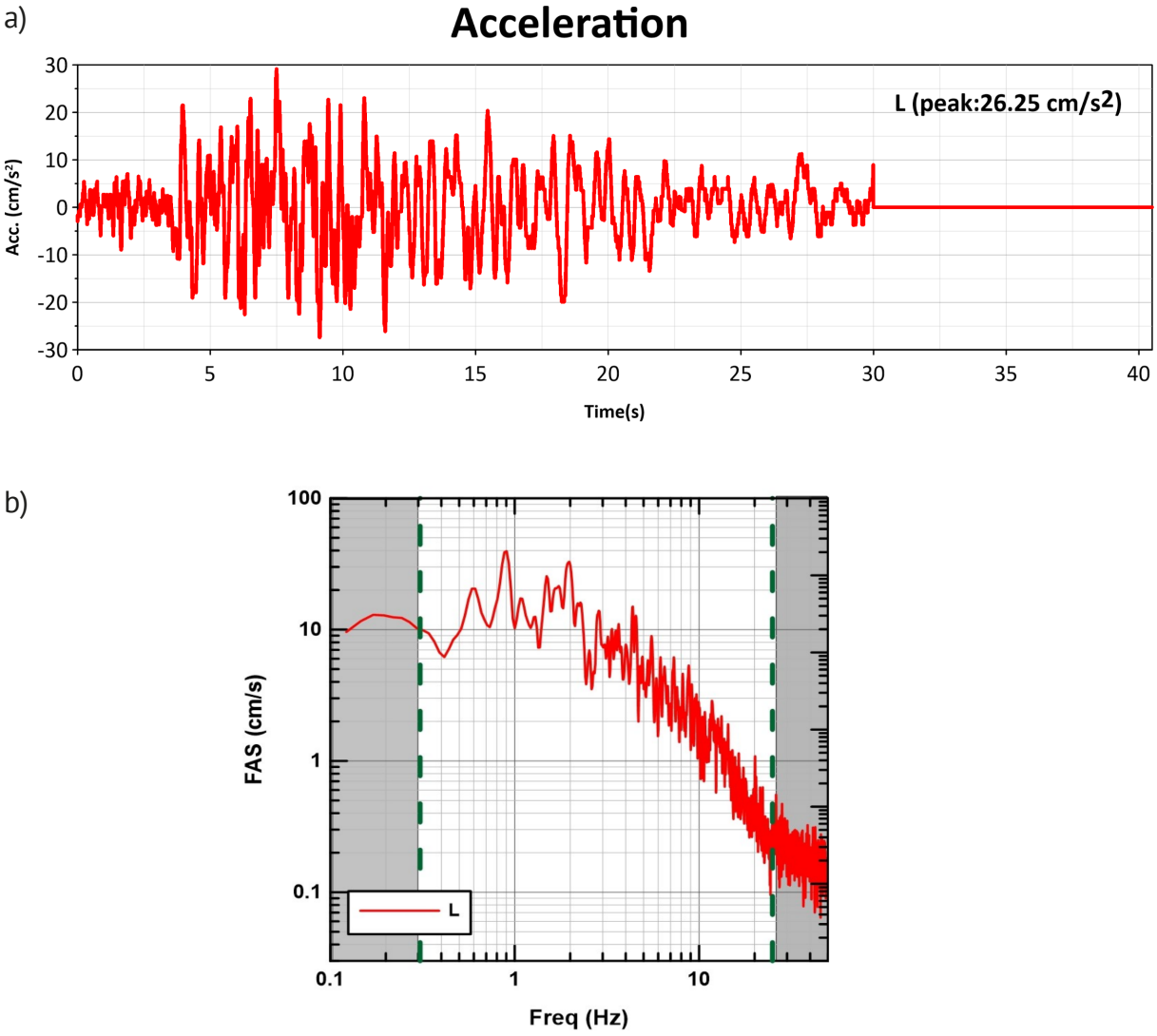

Figure 4. Observed recording of a horizontal component of station PAT3 (Patra) from the Aigio earthquake (**M**6.4, 1995): a) Ground-motion acceleration and, b) Fourier Amplitude Spectra (FAS). The useful frequency bandwidth, as determined from the record pre-processing and filtering, is depicted by vertical dashed lines.

3. Stochastic simulation of macroseismic data and strong motion FAS

To simulate both strong motion and macroseismic data, we applied the finite-fault stochastic simulation method with the use of the EXSIM algorithm, which is an open-source FORTRAN algorithm that generates time series of ground motion for earthquakes [Motazedian and Atkinson 2005; Boore, 2009; Atkinson et al., 2009]. In this approach, the adopted fault plane is divided into a grid of subsources, each of which is treated as a stochastic point source. The most important seismic source parameters taken into account by EXSIM (e.g., fault geometry of the considered seismic source, stress parameter, etc.) are summarized in Table 2 for all considered mainshocks. Since we are interested in the possibility to either automatize the process, or apply it for historical earthquakes (for which detailed seismic source information is usually not available) we have attempted to define almost all these parameters using generic, *a priori* information. More specifically:

a) The stress drop parameter was set to the default value of 70 bars proposed by Boore and Joyner [1997]. The value of 56 bars has been suggested for normal and strike-slip faults in Greece by Margaris and Boore [1998] and Margaris and Hatzidimitriou [2002]; as this value was based on a specific number of data, and since preliminary tests showed that it did not have a quantitatively significant effect on the simulated ground motion levels (in comparison to the "default" value), we kept the 70 bar value. A random-slip rupture pattern was adopted in the absence of alternative information, but also to maintain a "generic" modeling approach that could also be adopted for historical data.
b) The near-source crust's average shear wave velocity (β) was based on a near-source 1-D average calculated from the 3D model of Papazachos and Nolet [1997], while the density (ρ) was computed from appropriate Vs-ρ conversion relations [Boore, 2016]. The rupture propagation velocity, Vrup, was set to a typical value of 0.8β, and shear wave velocity (β) was set to 3.4 km/s [Benetatos and Kiratzi, 2006; Yolsal-Çevikbilen and Taymaz, 2012; Kkallas et al., 2018].
c) The fault's dimensions (length, L, and width, w) were estimated from the earthquake's moment magnitude, using equations (1) and (2), as proposed by Papazachos et al. [2004]. The dimensions of each subfault were also constrained from the magnitude of the event, using equation (3), proposed by Beresnev and Atkinson [1999].

$$\log L = 0.28M - 0.70 \quad (1)$$

$$\log w = 0.50M - 1.86 \quad (2)$$

$$\log \Delta l = 0.4M - 2 \quad (3)$$

d) The fault strike and dip were adopted from the published fault plane solution results (Table 1), while the depth of the top edge of the fault was constrained from the published focal depth, using the fault width, w, and dip angle, assuming that the epicenter is located at the fault's center. While this assumption is not always correct, it is a compromise which is necessary to perform automatized estimations when information on the detailed fault slip pattern is not available.
e) For the propagation model, information on the geometric spreading and anelastic attenuation is required. For the geometric attenuation the default geometric spreading was applied, which has been also shown to be appropriate for Greece [e.g. Roumelioti, 2004; Roumelioti et al., 2017; Kkallas et al., 2018; Giannaraki et al., 2019]. Moreover, the anelastic attenuation was constrained by a mean frequency-dependent quality factor, $Q(f) = 100f^{0.8}$, proposed for the broader Aegean Sea by Hatzidimitriou (1993, 1995).

An important factor for the simulations is the assessment of site-effect on seismic motions. It should be mentioned that site conditions (local geology, Vs_{30} value, etc.) for macroseismic observations are usually not known, especially for historical earthquakes. For this reason, we employed the SRTM3 morphological model to determine Vs_{30} values from slope proxies, following Wald and Allen, [2007]. This approach has been shown to be suitable for a semi-em-

Parameter	Earthquake			
	Alkyonides (24/02/1981, M = 6.7)	Kalamata (13/09/1986, M = 6.0)	Kozani (13/05/1995, M = 6.6)	Aigio (15/06/1995, M = 6.4)
Strike	264°	200°	240°	276°
Dip	42°	50°	45°	33°
L	30.9 km	13.8 km	27.5 km	21.9 km
W	15.0 km	9.5 km	14.1 km	12.4 km
Ztop	0.0 km	2.9 km	1.0 km	3.3 km
NL × NW	6 × 3	5 × 4	6 × 3	6 × 3
dL	5.16 km	2.80 km	4.66 km	3.66 km
Dw	5.00 km	2.50 km	4.66 km	4.00 km

Table 2. Seismic source parameters for the application of the finite-fault stochastic method for the Alkyonides, Kalamata, Kozani and Aigio earthquakes [Papazachos and Papazachou, 1997].

pirical Vs_{30} assessment from topographic slope data for the Europe and Greece [Lemoine et al., 2012; Stewart et al., 2014], and has been successfully applied for intermediate-depth events in Greece (Kkallas et al., 2018]. Using the determined Vs_{30} value from the previous process, soil classes according to NEHRP (1994) have been assigned to each site for which simulations were performed (IDP site). Following this classification, generic transfer site amplification functions for NEHRP site conditions A/B, C and D, were adopted from the work of Margaris and Boore [1998] and Klimis et al. [1999] and were used in all simulations with the EXSIM code, to account for the contribution of site-effects. Table 3 summarizes all the parameters employed for the site-effect classification, including the Vs_{30} velocity classification, and the empirically derived kappa-0 (k_0) high-frequency attenuation value that were adopted. Figure 5 presents the final generic site- amplification curves used for each soil class.

NEHRP class	Soil profile	Vs_{30} (m/s)	k_0	References
A/B	Rock/Hard rock	$760 \leq Vs_{30} \leq 1500$	0.035	Margaris and Boore (1998)
C	Very dense soil and soft rock	$360 \leq Vs_{30} \leq 760$	0.044	Klimis et al. (1999)
D	Stiff soil	$180 \leq Vs_{30} \leq 360$	0.066	Klimis et al. (1999)

Table 3. High frequency attenuation parameter k_0 and Vs_{30} values for the NEHRP classification adopted for each soil class in the simulations.

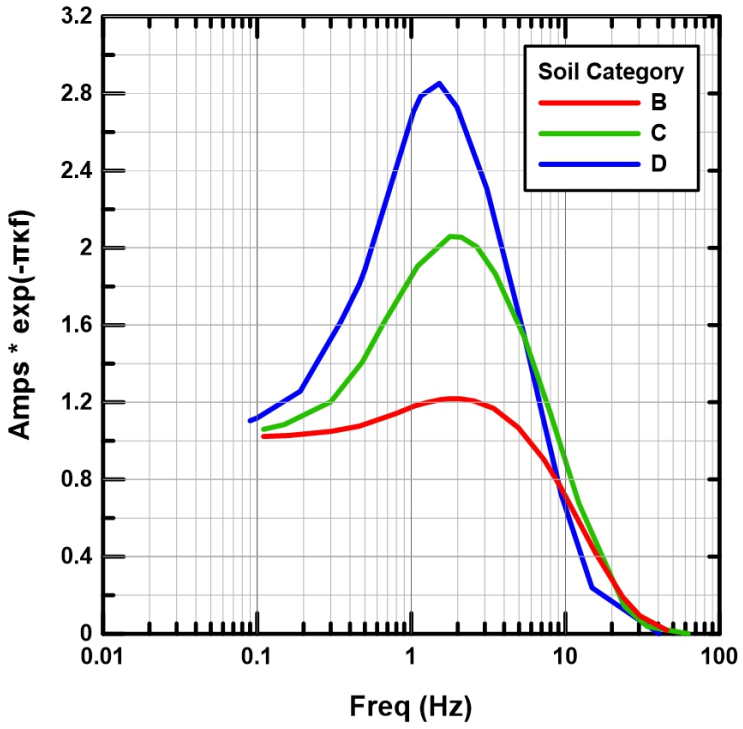

Figure 5. Generic amplification functions (combined effect of amplification and high-frequency attenuation) for the area of Greece [information from Margaris and Boore, 1998 and Klimis et al., 1999]. The amplification term is based on the quarter-wavelength approximation, while the high-frequency attenuation is expressed as $\exp(-\pi k_0 f)$, where k_0 values are determined according to each site class (B, C or D).

Simulated seismic motions for the considered four mainshocks needed to be converted into macroseismic intensities, to be compared with the available IDP data. We have adopted a simple approach, where the PGA and PGV values from the synthetic waveforms were converted into macroseismic intensities (Modified Mercalli scale, I_{MM}, as adapted in Greece). For this conversion we used the relations proposed by Kkallas et al. [2018], who proposed an adapted version of the Wald et al. [1999] relation, accounting for the bias of the Greek version of the Modified Mercalli scale macroseismic scale [Shebalin, 1974; Papazachos and Papaioannou, 1997], as given by equations (4) to (7).

$$I_{MM} = 2.10 \log_{10}\left(\frac{PGV}{5.8}\right) + 5.5 \qquad 0.37 \leq PGV\ (cm/s) < 5.8 \tag{4}$$

$$I_{MM} = 3.47 \log_{10}\left(\frac{PGV}{5.8}\right) + 5.5 \qquad PGV\ (cm/s) \geq 5.8 \tag{5}$$

$$I_{MM} = 2.20 \log_{10}\left(\frac{PGV}{66}\right) + 5.5 \qquad 4.8 \leq PGA\ (cm/s^2) < 66 \tag{6}$$

$$I_{MM} = 3.66 \log_{10}\left(\frac{PGV}{66}\right) + 5.5 \qquad PGA\ (cm/s^2) \geq 66 \tag{7}$$

The Fourier Amplitude Spectra of synthetic acceleration time histories computed from EXSIM were also employed for a direct comparison with the observed strong motion data. For these synthetic seismograms the local site-effects were constrained using information provided in the HEAD database. It should be noticed that all spectral comparisons between real (observed) and synthetic (modeled) waveforms were performed for the FAS window for which the observed FAS was reliable, as this is indicatively depicted in Figure 4 for a typical acceleration record.

4. Simulation of the 1981 Alkyonides earthquake (24/02/1981, M = 6.7)

The Corinth Gulf is one of the most important seismotectonic zones in the Aegean area, due to its high seismicity and impressive extensional tectonics, often considered as one of the largest fracture zones in the world and associated with N-S extension at a rate of 10-14 mm/yr [Briole et al., 2000]. It is an asymmetric half-graben, with an uplifted southern coast and a submerged northern one [Armijo et al. 1996; Papanastassiou, 2002]. The most active normal faults of the rift are dipping north, resulting in a long-term subsidence of the northern coast and an upward displacement of the footwalls [Armijo et al. 1996; Console et al, 2015]. The Alkyonides mainshock epicenter (**M**6.7) was located in the western coast of the Corinth Gulf and occurred along the northern coast of the Perachora peninsula. The aftershock activity migrated eastwards, with a very strong aftershock (**M**6.4) which occurred less than 6 hours after the mainshock, and a second strong aftershock (**M**6.3) which occurred 8 days later, in the Platees area, beyond the eastern end of the gulf [Jackson et al., 1982; Mariolakos et al., 1982; Karakaisis et al., 1985; Papazachos and Papazachou, 1997].

The collected macroseismic data for this earthquake included observed macroseismic intensities (I_{MM} values) ranging from 3 to 9.5 for 997 settlements, located at various site geological conditions (rock, soft rock/stiff soil and soft soil formations). The heaviest damage was observed in Perachora (IX+), Pisia, Schinos (IX) Loutraki (VIII+), Kiato, Pasio, Xylokastro, Moulkio, Karya, Velo (VIII) of Corinthia, Prodromos (IX+), Koryni, Thisvi (VIII+) Mauromati, Vagia (VIII) of Boeotia and Megara (VIII) of Attica [Papazachos and Papazachou, 1997]. It is worth to notice that this earthquake had also an important economic and social impact in the metropolitan area of Athens. Moreover, its damage cannot be discriminated from its largest aftershock, as both events occurred during the night of 24 February and the collected macroseismic information (which occurred during the following days) concerns the accumulated effect of both (**M**6.7 and **M**6.4) events. In total, 22554 buildings collapsed or suffered non-repairable damage, 11745 suffered severe damage and 50222 suffered medium-level damage [Papazachos and Papazachou, 1997]. Furthermore, 20 human losses and more than 500 injuries were also reported (Papazachos and Papazachou, 1997].

In Figure 6 we present the adopted fault geometry (upper fault edge) for the simulations, the IDP with $I_{MM} \geq$ VIII [Papazachos and Papazachou, 1997] and the mapped surface faulting traces, as summarized by Abercrombie et al. [1995]. It is clear the coincidence in Figure 7 we show the spatial variation of the synthetic (top) and observed (bottom) distribution of macroseismic intensities. A good agreement of the spatial distribution of reported and syn-

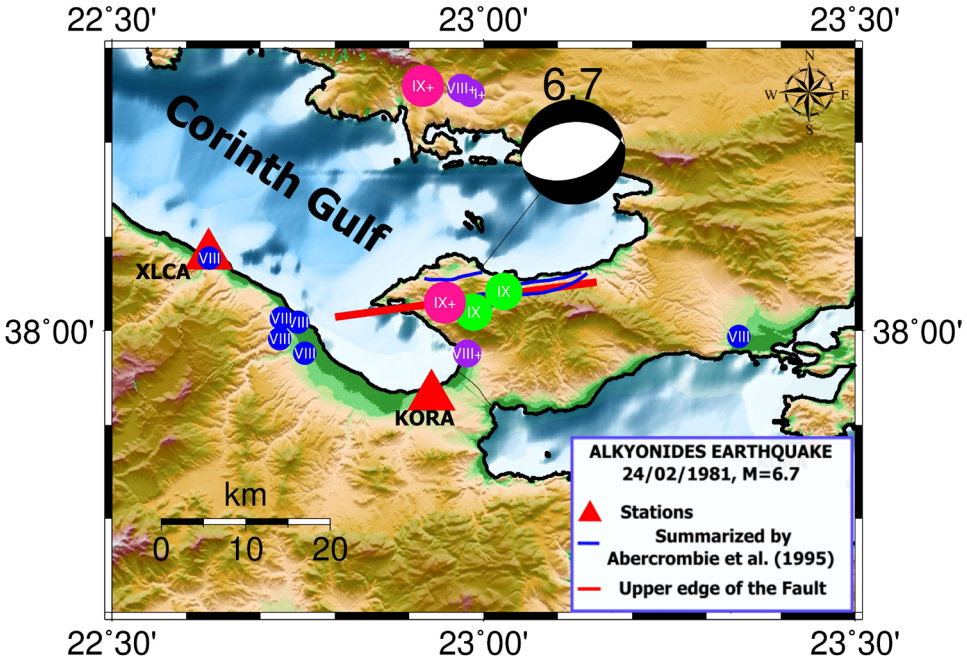

Figure 6. Fault model (upper fault edge) used to simulate the Alkyonides earthquake damage pattern (1981, **M**6.7). The focal mechanism, the stations for which strong motion records were used (red triangles), as well as main surface faulting traces observed after the earthquake in the study area by various authors (as summarized by Abercrombie et al., 1995) are also depicted. Sites with $I_{MM} \geq$ VIII are also shown.

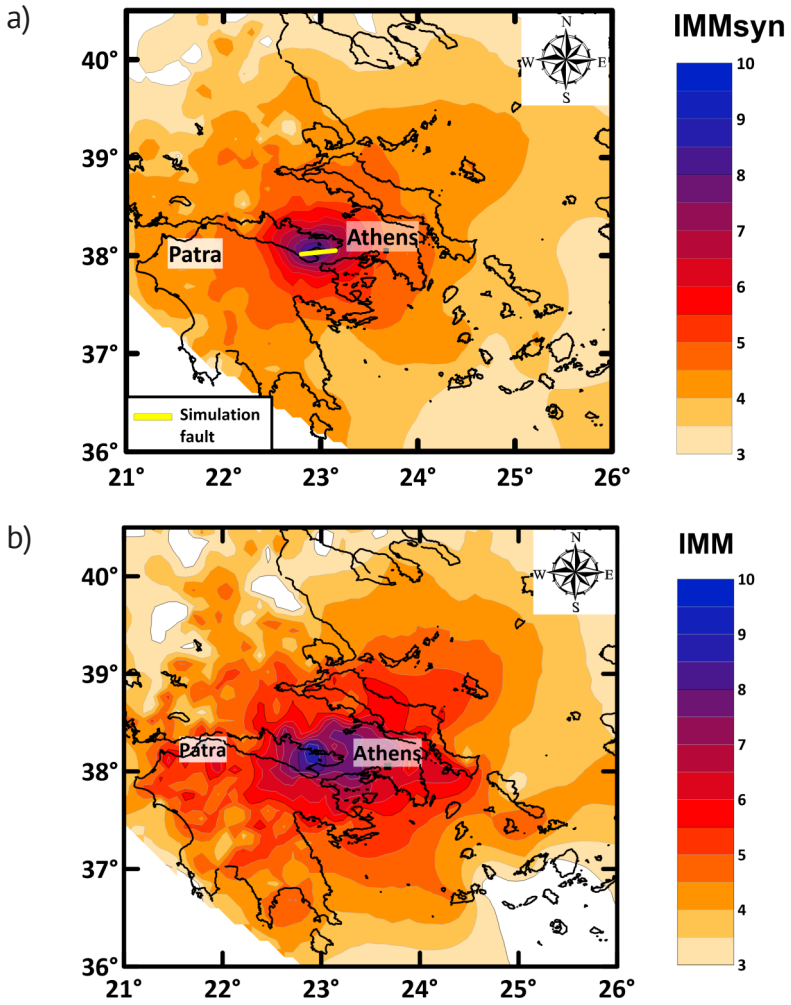

Figure 7. Spatial distribution of synthetic (a) and observed (b) I_{MM} values for the Alkyonides earthquake (24/02/1981, **M**6.7). The upper fault edge is depicted with a yellow solid line in (a).

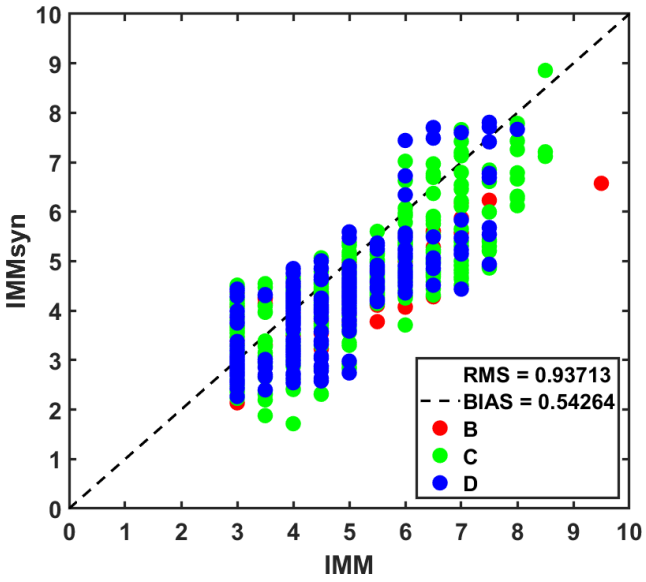

Figure 8. Comparison of the modelled (synthetic), IMMsyn, against observed, IMM, macroseismic intensities for the Alkyonides earthquake (24/02/1981, **M**6.7) using the EXSIM code (red circles for rock – B class, green circles for stiff soil – C class, blue circles for soft soil– D class).

thetic macroseismic intensities is observed, showing that were able to reconstruct the main features of the damage distribution, with a rather generic, semi-automatic simulation approach. However, the observed I_{MM} values are generally larger than the synthetic ones, most probably due to the combined damage effect of the mainshock and its largest aftershock, that could not be separated in the original macroseismic observations. This is confirmed by the plot presented in Figure 8, where we also observe a significant deviation between observed and synthetic macroseismic intensities: The results show a large positive bias (roughly half intensity unit) between observed and predicted intensities and a very larger RMS misfit (almost 1 intensity unit). Notice that this is not a result of the generic site-effect assessment, as the distribution of synthetic and observed I_{MM} values does not seem to vary with the adopted soil class for all available IDP points.

5. Simulation of the 1986 Kalamata earthquake (13/09/1986, M = 6.0)

The **M**6.0 1986 Kalamata earthquake was caused by a normal fault, with strike about N195° and a dip of ~50° [Lyon Caen et al., 1988; Papazachos et al., 1988]. The mainshock was followed by several aftershocks, the strongest of which had a moment magnitude of **M**5.4. The observed surface coseismic displacement on the fault trace ranged between 6 and 18 cm. The seismic sequence of Kalamata caused severe damage not only in the city of Kalamata, but also in the eastern extension of the Kalamata area (Giannitsanika district). Moreover, the maximum values of the macroseismic intensities were observed along at the whole rupture zone. The collected macroseismic data for this earthquake (I_{MM} values) ranged from 3 to 8 for 424 settlements. The heaviest damage was observed in the settlements of Elaeochori, Verga (VIII), Poliani (VII+), Aris, Artemisia and Nedousa (VII) [Papazachos and Papazachou, 1997].

Concerning the simulation model, we considered not only the focal mechanism solution [Papazachos and Papazachou, 1997] but also several papers published for this event. In Figure 9, we present the fault geometry (upper fault edge) adopted for the simulations, (red thick line) sites with $I_{MM} \geq$ VII, as well as surface fault traces summarized by other researchers [Lyon-Caen et al., 1988; Papazachos et al., 1988; Kazantzidou-Firtinidou et al.,

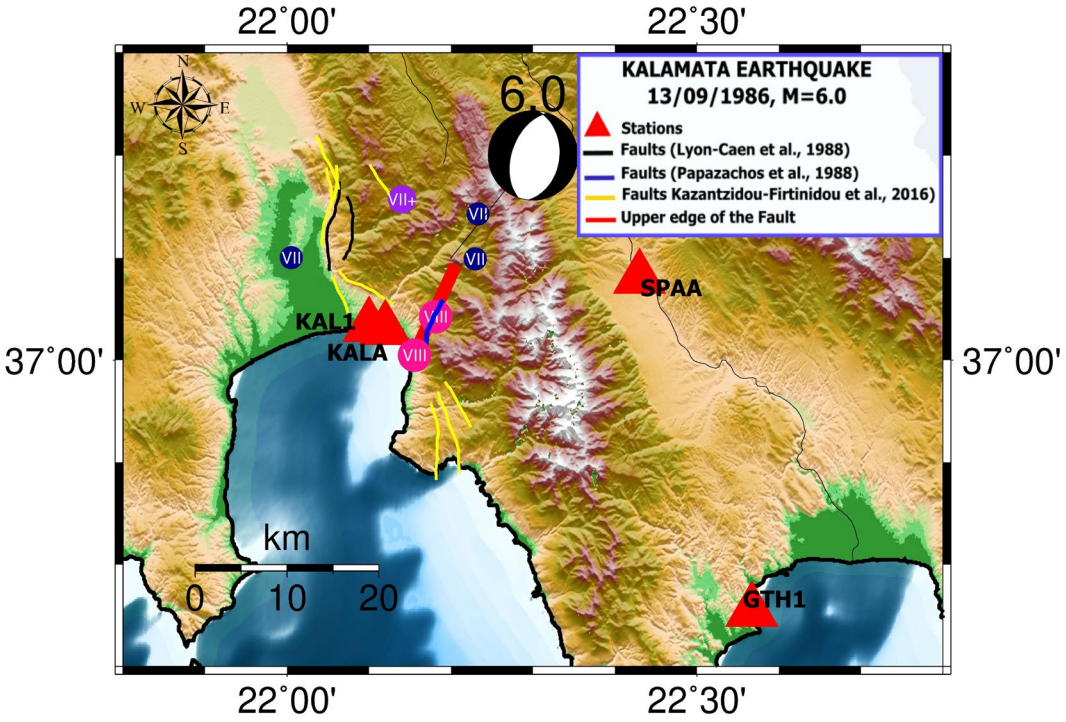

Figure 9. Fault model (upper fault edge) used to simulate the 1986 **M**6.0 Kalamata earthquake damage pattern. The focal mechanism, the stations for which strong motion records were used (red triangles), as well as main surface faulting traces observed after the earthquake in the study area by various authors are also depicted. Sites with $I_{MM} \geq$ VIII are also shown.

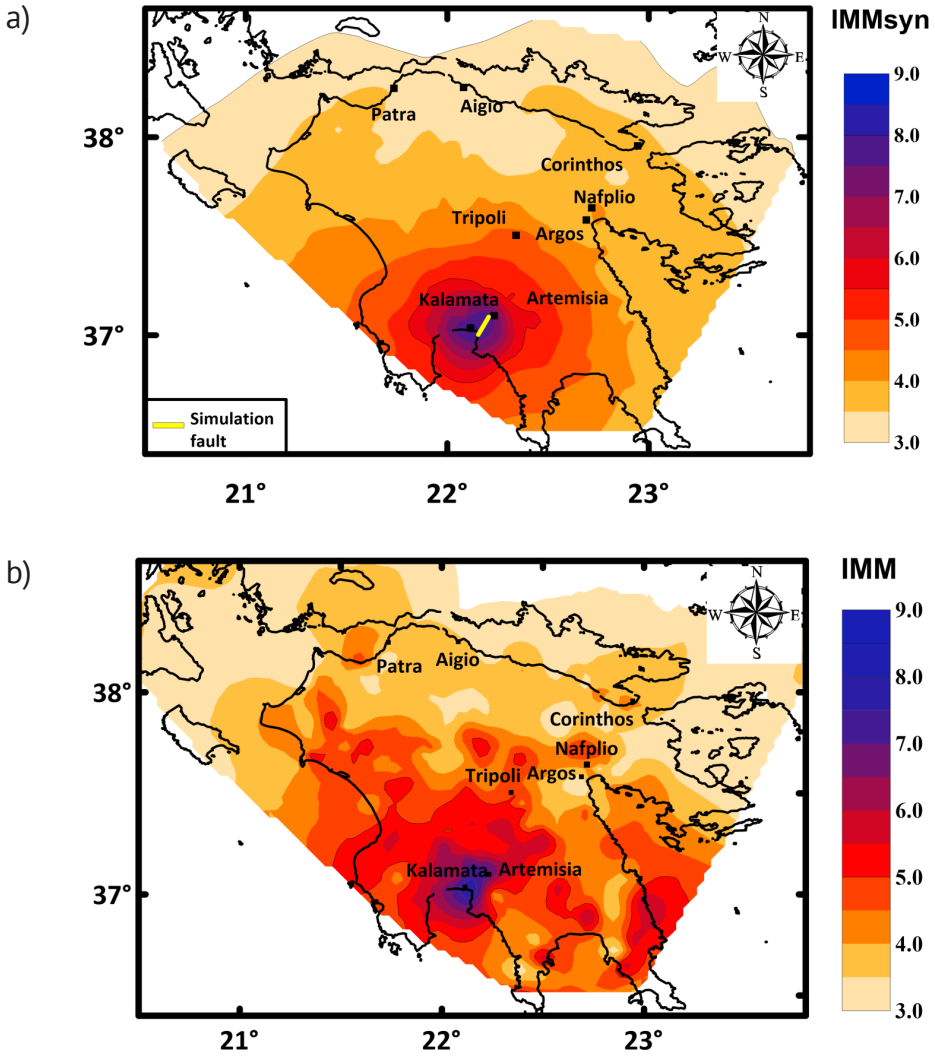

Figure 10. Spatial distribution of synthetic (a) and observed (b) I_{MM} values for the 1986 Kalamata earthquake (**M**6.0). The upper fault edge is depicted with a yellow solid line in (a).

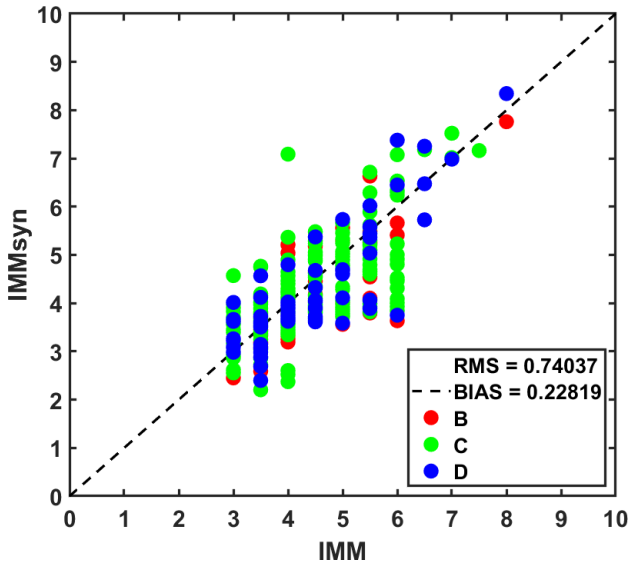

Figure 11. Comparison of the modelled (synthetic), IMMsyn, against observed, IMM, macroseismic intensities for the Kalamata earthquake (13/09/1986, **M**6.0) using the EXSIM code (notation is same with Figure 8).

2016]. Notice the good agreement between the mapped faults in the epicentral area and the representation of the seismic fault used in the calculations. Furthermore, in the same figure all stations that recorded the strong ground motion are depicted, namely GTH1 (Githio), KAL1-KALA (Kalamata) and SPAA (Sparta). In Figure 10 we present the spatial pattern of the synthetic (top) and the observed (bottom) distribution of macroseismic intensities. The results for higher intensity levels ($I_{MM} > VI+$) show a good agreement between modelled and observed intensities, while for lower intensities a rather small positive bias between observed and predicted intensities is observed, i.e., the actual damages are rather larger than those predicted. This is evident also in Figure 11, where we compare observed and modeled I_{MM} values, where a positive bias of ~0.2 intensity units and a large RMS misfit (0.7-0.8) is seen. Therefore, while we were able to reconstruct the main features of the damage distribution close to the fault, the results suggest that we rather underestimate the I_{MM} values at larger epicentral distances. This can be due to several reasons, such as weaker attenuation of seismic energy with distance, site amplifications (e.g., deep basin effects in western Peloponnesus), as well as other factors (e.g., source-slip distribution) not accounted by the generic modeling approach adopted here, where most model parameters were automatically calibrated on the basis of *a priori* information.

6. Simulation of the 1995 Kozani earthquake (13/05/1995, M = 6.6)

Kozani is located at the western part of Hellinides at the NW Greece, where the NW-SE extension observed along western Greece prevails. The seismic sequence caused significant damage in Grevena and Kozani cities. Several researchers suggest that the fault is normal, with a strike of ~240° and a dip of ~40° to the north-northwest [Papazachos et al., 1996; Meyer et al., 1996; Hatzfeld et al., 1997; Kiratzi, 1999; Ding et al., 2019]. According to Papazachos and Papazachou [1997], the mainshock was preceded by foreshocks, the largest of which occurred 4 minutes before (08:43, **M**4.5) and was followed by several aftershocks, the largest of which occurred in 17/07/1995 (23:18, **M**5.5).

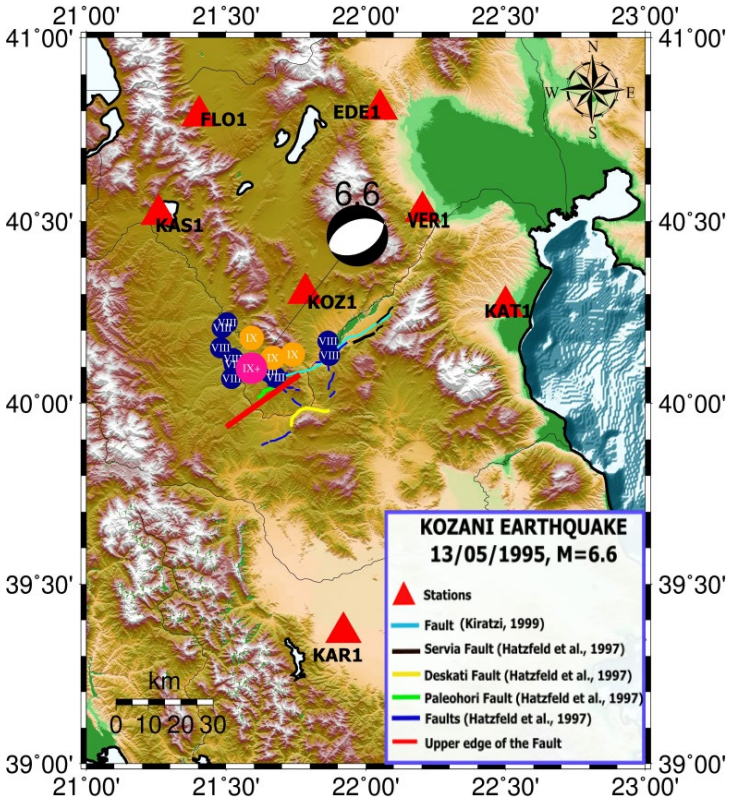

Figure 12. Fault model (upper fault edge) used to simulate the 1995 **M**6.6 Kozani earthquake damage pattern. The focal mechanism, the stations for which strong motion records were used (red triangles), as well as main surface faulting traces observed after the earthquake in the study area by various authors are also depicted. Sites with $I_{MM} \geq$ VIII are also shown.

Along the rupture zone of total length of 30 km, where the maximum values of macroseismic intensities were reported ($I_{MM} > VIII$), ground fissures of up to 15 km length, with an ENE-WSW direction were also observed. The heaviest damages were reported not only for the Grevena prefecture (Knidi (IX+), Kalamitsi, Varis (IX), Taxiarches, Kokkinia, Vatolakkos, Poros, Lanadakia, Kalochio, Pyliroi and Pontine (VIII) but also for the broader Kozani area (Chromio, Daphnero (IX), Podiane, Kaesareia, Rymnio (VIII). More specifically, in Grevena a total number of 1924 buildings collapsed, while 1599 were serious damaged. Moreover, in Kozani prefecture the total number of collapsed structures was equal to 7693. The collected macroseismic data for this earthquake included observed macroseismic intensities (I_{MM}) ranging from 3 to 9.5 for 607 settlements.

The strong ground motion from the 1995 Kozani-Grevena earthquake was studied by Ding et al. [2019] using a hybrid deterministic-stochastic approach. An alternative approach was adopted by Roumelioti et al. [2000], who presented a comparative study (deterministic and stochastic) simulation of strong ground motions for the 1995 Kozani sequence.

In Figure 12, we present the adopted fault geometry (upper fault edge) for the simulations, and surface fault traces, as given by various studies previously mentioned. The representation of the fault adopted for the calculations is in perfect agreement with the mapped fault traces from field investigations. Also, in the same figure, the location of the stations EDE1 (Edessa), FLO1 (Florina), KAR1 (Karditsa), KAS1 (Kastoria), KAT1 (Katerini), KOZ1 (Kozani) and VER1 (Veria) that recorded the strong ground motion and sites with $I_{MM} \geq VIII$ are also depicted (red

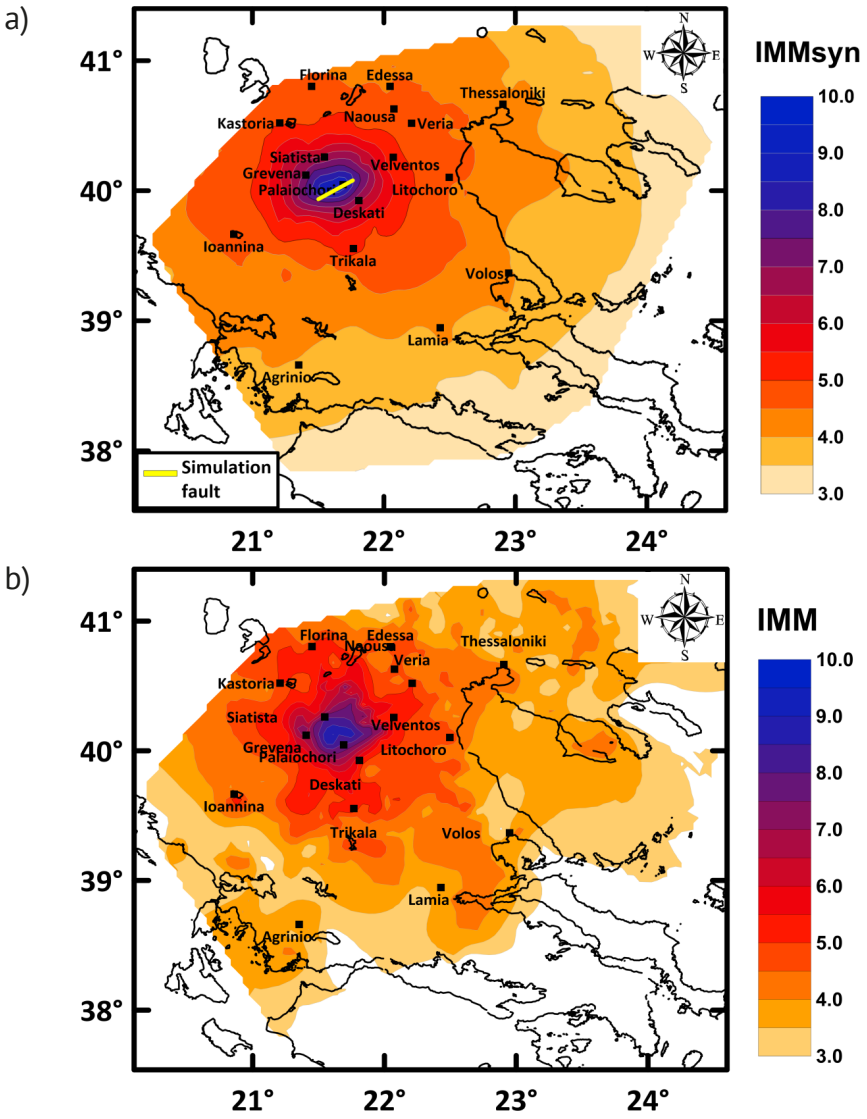

Figure 13. Spatial distribution of synthetic (a) and observed (b) I_{MM} values for Kozani earthquake (1995, **M**6.6). The thick light yellow line in (a) represents the upper fault edge.

triangles and colored circles respectively). The preferred model used in simulation had an upper fault edge depth of ~1 km. In Figure 13 we show the spatial variation of the synthetic (top) and observed (bottom) distribution of macroseismic intensities for this earthquake. In Figure 14 the calculated synthetic macroseismic intensities are plotted versus the observed values. The highest observed intensity values were observed at villages of the two prefectures, where the typical construction system was rather poor, resulting in heavy damage degree (high intensity values), which cannot be predicted by simple empirical relations. Overall, Figure 14 shows a small negative bias between observed and predicted intensities, with a rather small RMS misfit (~0.6 intensity units), comparable to the typical observed intensity determination error of half intensity unit.

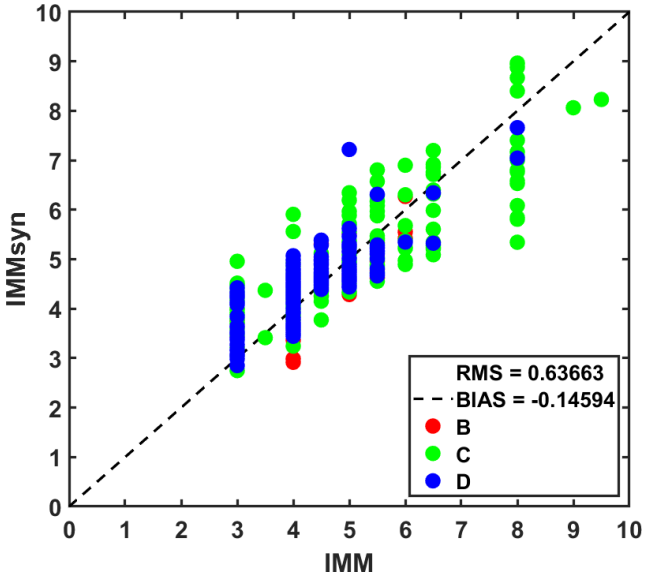

Figure 14. Comparison of the modelled (synthetic), IMMsyn, against observed, IMM, macroseismic intensities for the Kozani earthquake (13/05/1995, M6.6) using the EXSIM code (notation is same with Figure 8). See text for details.

7. Simulation of the 1995 Aigio earthquake (06/15/1995, M = 6.4)

The Aigio 1995 mainshock (**M**6.4) was preceded by many foreshocks, the largest of which occurred at 28/05/1995 (19:56, **M**4.6), and was followed by a large number of aftershocks, the largest of which occurred 15 minutes after the mainshock (00:31, **M**5.6) [Papazachos and Papazachou, 1997]. The collected macroseismic data for this earthquake included observed macroseismic intensities (I_{MM}) ranging from 3 to 8 for 409 settlements. The earthquake mainly affected Aigio (I_{MM}=VIII), Valimitika (Achaia, VII) and Phokida (VII, Erateini and Tolophon). Concerning the consequences of the earthquake in Aigio, 1071 buildings suffered major and 996 minor damage, while in neighboring villages 778 buildings suffered major and 760 minor damage. Finally, 3 buildings collapsed (one in Aigio, a hotel in Valimitika and a partial collapse of the Hellenic Defense Systems industrial complex). There were also 26 human losses.

For the simulation scenario we also considered results obtained by the use of broadband strong ground motion modeling [Mavroeidis et al., 2018] and deterministic seismic risk assessment [Giannaraki et al., 2019]. In Figure 15, we present the adopted fault geometry (upper fault edge) for the simulations, sites with $I_{MM} \geq$ VII and other active faults given by Bernard et al. [1997]. In the same figure, the stations that recorded the strong ground motion of Aigio earthquake are given: AIGA (Aigio), AMIA (Amfissa), MRNA (Mornos), NAUA (Naupaktos) and PAT1-PAT2-PAT3-PATA (Patra). In Figure 16 we show the spatial variation of the synthetic (top) and observed (bottom) distribution of macroseismic intensities for this event. Finally, in Figure 17 the comparison between observed and synthetic macroseismic intensities is shown. The observed intensities show a good agreement with the results of the stochastic simulation (RMS misfit between modeled and synthetic data ~0.6 intensity units), though for the adopted simulation scenario the corresponding synthetic I_{MM} values slightly overestimate the actual damage distribution (bias of roughly –0.3 intensity units).

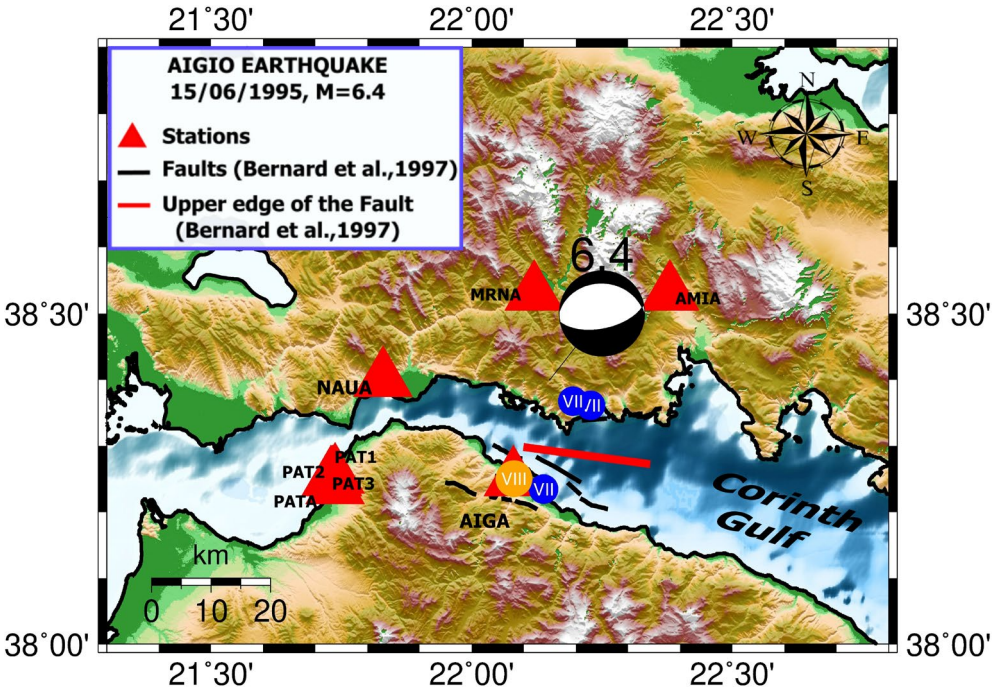

Figure 15. Fault model (upper fault edge) used to simulate the 1995 **M**6.4 Aigio earthquake damage pattern. The focal mechanism, the stations for which strong motion records were used (red triangles), as well as the main active faults in the broader study area reported by Bernard et al. [1997], are also presented. Sites with $I_{MM} \geq$ VII are also shown.

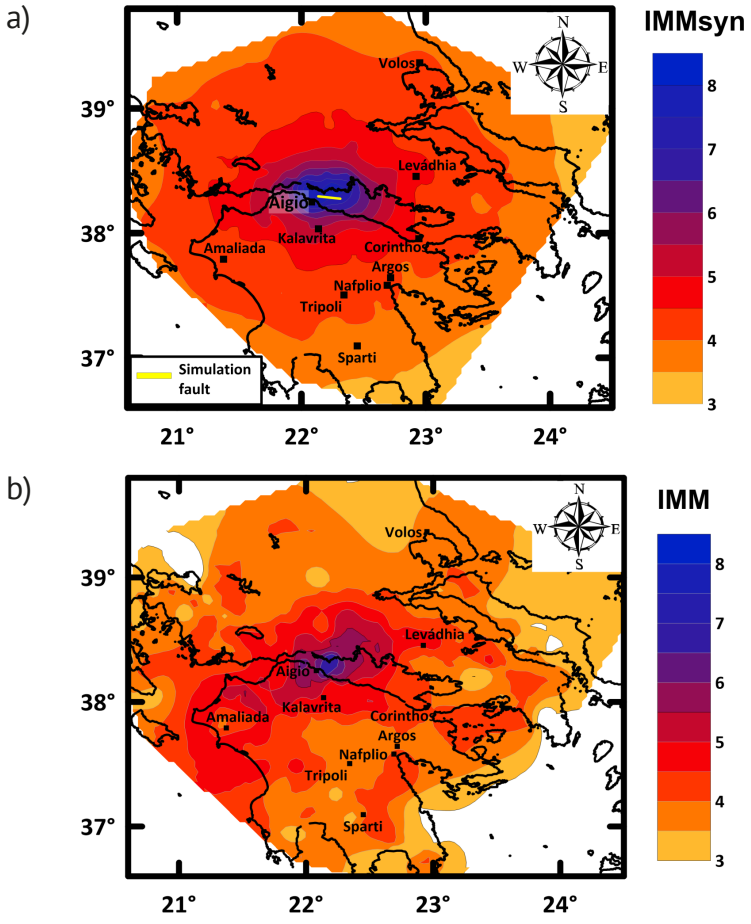

Figure 16. Spatial distribution of the synthetic (a) and observed (b) I_{MM} values using the EXSIM code for the Aigio earthquake (15/06/1995, **M**6.4). The fault plane (upper fault edge) is depicted with yellow solid line in (a).

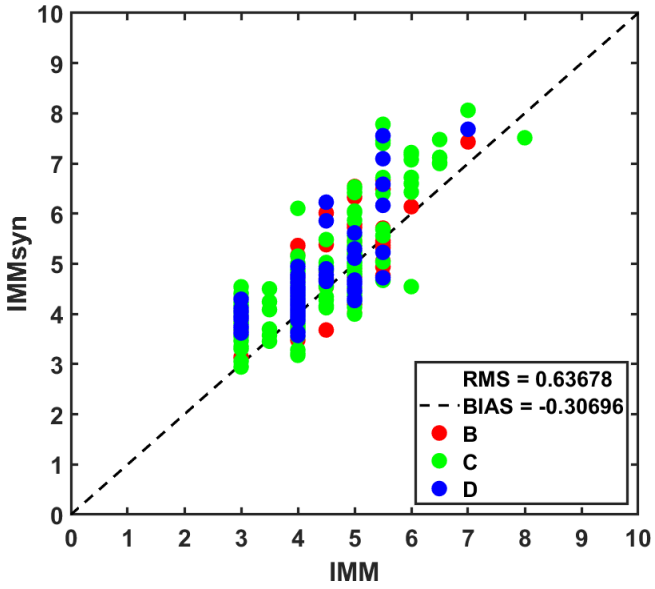

Figure 17. Comparison of the modelled (synthetic), IMMsyn, against observed, IMM, macroseismic intensities for Aigio earthquake (15/06/1995, **M**6.4) using the EXSIM code (red solid circle for rock – B class, green solid circle for dense soil – C class and blue solid circle for stiff soil– D class).

8. Simulation of FAS for strong motion

For all previous studied earthquakes, we also employed the available strong motion data from strong motion stations for each earthquake. Fourier Amplitude Spectra (FAS) from the available station records were computed and compared with the synthetic Fourier Amplitude Spectra determined from the stochastic simulation. For both observed and synthetic data we also took into account the bandwidth range determined during the filtering process of each strong motion waveform, separately. In Figure 18 we present indicative comparisons for two selected recording stations of each one of the earthquakes considered. Specifically, the two horizontal components (L- and T-) of the selected recording stations are compared with the simulated Fourier Amplitude Spectrum that was derived from the use of the EXSIM algorithm. Table 4 summarizes the information for stations who are presented for each earthquake (Latitude, Longitude, Soil type), as well as the low-cut frequency (f_{low}) employed in the pre-processing band-pass filter (the high-cut limit was set to 25Hz in all cases).

Station Code	Earthquake	Latitude	Longitude	Soil type (NEHRP)	f_{low} (Hz)
AIGA	Aigio (15/06/1995, **M**6.4)	38.250	22.080	C	0.500
PAT3	Aigio (15/06/1995, **M**6.4)	38.254	21.738	D	0.307
XLCA	Alkyonides (24/02/1981, **M**6.7)	38.080	22.630	D	0.125
KORA	Alkyonides (24/02/1981, **M**6.7)	37.930	22.930	D	0.572
SPAA	Kalamata (13/09/1986, **M**6.0)	37.080	22.430	C	0.362
KAL1	Kalamata (13/09/1986, **M**6.0)	37.033	22.100	C	0.307
FLO1	Kozani (13/05/1995, **M**6.5)	40.787	21.404	B	1.279
KOZ1	Kozani (13/05/1995, **M**6.5)	40.302	21.784	B	0.656

Table 4. Information on strong motion stations and records for each earthquake considered in the present work.

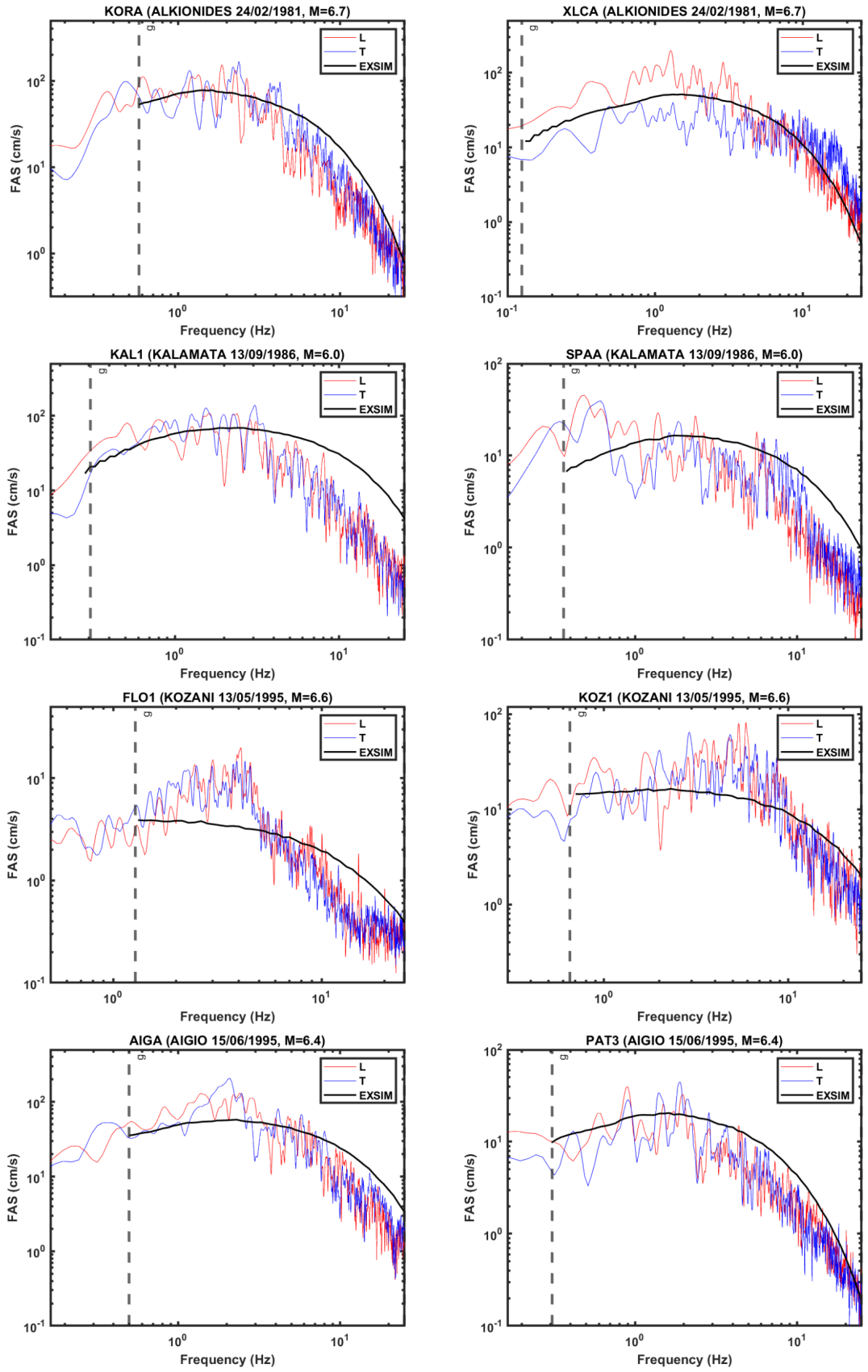

Figure 18. Fourier Amplitude Spectrum (FAS) of the two observed horizontal components of selected stations for the earthquakes of Alkyonides (24/02/1981, **M**6.7), Kalamata (13/09/1986, **M**6.0), Kozani (13/05/1995, **M**6.6) and Aigio (15/06/1995, **M**6.4). In the same plot, the Fourier Amplitude Spectra from stochastic simulations (EXSIMblack solid line) is depicted for the simulation scenario of each earthquake (Table 2). The low-cut reliability limit of each FAS record, as determined from the strong-motion filtering process, is depicted with a grey dashed line.

The comparison shows that the FAS of the strong motion data were adequately matched (in most cases) by the synthetic data from the EXSIM simulations. This is evident for the Alkyonides (1981, **M**6.7) and Aigio (1995, **M**6.4) events, where a good correlation of observed and recorded FAS is identified for the whole spectral range. This observation is especially important for the Alkyonides 1981 mainshock: While the observed macroseismic data comparison (Figure 8) shows that we cannot match the observed damages, the FAS comparison is more than adequate, considering that it is a result of semi-automated modeling. This confirms our previous suggestion that the damage observations of the 1981 mainshock were further amplified by the combine effect of its large aftershock that followed within a few hours. This has important implications for the simulation of similar historical earthquakes, where increased damages from similar multiple events may lead to an overestimation of the "mainshock" magnitude.

FAS comparisons for the other two earthquakes show poorer correlations. For the Kalamata **M**6.0 event the high-frequency content is not properly modelled in both cases considered in Figure 18, most probably due to the generic (and not necessarily locally representative) value used for the high-frequency attenuation factor, k_0. For the Kozani 1995 **M**6.5 event, a larger misfit is also observed also for intermediate frequencies (e.g., for the FLO1 record), showing that the employed semi-automated process has certain limitations, as it cannot capture event-specific effects (due to e.g., specific fault-slip pattern, directivity, etc.).

The FAS comparisons presented in Figure 18 provide interesting information on the spectral content of the simulations, such as specifying ground motion characteristics in engineering seismology. It is often adequate (and necessary) to be able to model the corresponding observed peak ground motion values, as they are more easily collected by acquisition systems, but also indirectly assessed from field observations (e.g., liquefaction, static displacement observations, etc.), even for historical events. For this reason, we have also compared the observed and synthetic PGA and PGV values for all recording stations available for the four (4) considered events. To enrich the dataset, we have also included seven (7) additional PGA and PGV comparisons from simulation results obtained with the same approach for the earthquakes of Stivos (1978, **M**6.5) and Kyllini (1988, **M**6.0), as reported by Ravnalis [2020].

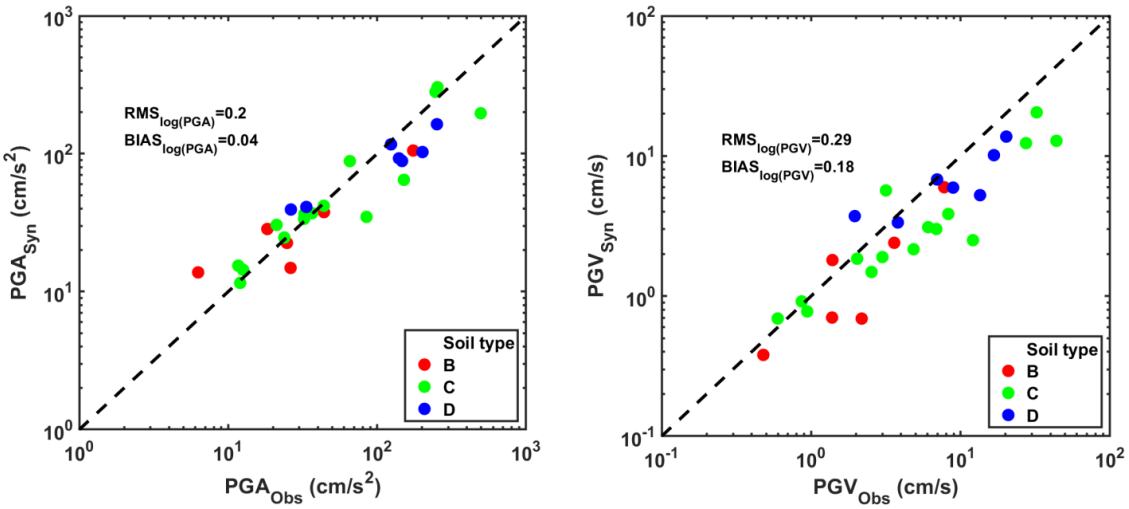

Figure 19. Correlation between observed and synthetic PGA (left) and PGV values (right), for each soil type category (NEHRP classification). The equality line (depicted by a dashed line), as well as the bias and RMS misfit between the logarithms of peak ground motions, are shown in both figures.

The comparison is presented in Figure 19, using the adopted NEHRP soil classification for each observation/simulation pair. In general, a very good correlation is observed in both cases, especially for the PGA values, considering the small, estimated bias between modeled and observed values, as well as the low RMS misfits between the logarithm of observed and synthetic PGA and PGV values. Both the bias and the estimated RMS misfits suggest a poorer fit for the PGA values, in comparison to PGA. It should be also noticed that class D (soft soil) and class A/B (rock) sites seem be cluster closer to the equality line for both PGA and PGV, with the C class sites are showing a rather larger spread, especially for PGV. This is pattern is rather expected, as low-frequency amplifications often observed

for e.g., deep basin sites, that mostly affect the PGV values, cannot be properly captured by the generic site-amplification transfer functions adopted in this work (shown in Figure 5). On the other hand, the good correlation of observed and synthetic peak ground motions in Figure 19 verifies that employed stochastic finite-fault modeling can be reliably applied for strong motion data simulations, even in the semi-automated approach adopted in this work.

9. Summary and Conclusions

The aim of this work was to perform a simultaneous interpretation of two types of data (namely macroseismic and strong motion data) for four shallow normal faulting earthquakes with **M** ≥ 6.0 Alkyonides (24/02/1981, **M**6.7), Kalamata (13/09/1986, **M**6.0), Kozani (13/05/1995, **M**6.6) and Aigio (15/06/1995, **M**6.4), that occurred in the period 1980-1995, for which both macroseismic intensities and strong motion recordings were available. The method of finite-fault stochastic simulation of strong ground motion (EXSIM) was applied to produce synthetic time series records and reconstruct the spatial distribution of strong ground motion in all cases. By applying appropriate, adapted scaling relations [Wald et al., 1999; Kkallas et al., 2018] and converting synthetic PGA and PGV values (from stochastic simulation) to macroseismic intensity, a comparison with the actual (observed) macroseismic data was performed. The majority of the parameters employed for the stochastic simulation were automatically assigned, in an attempt to fully automatize the process (e.g., to be employed for historical earthquake assessment). A better data fit could be obtained for all events by adopting additional optimization of individual model parameters, related to the seismic source (e.g., different stress parameter for each event), propagation path (e.g., different velocity or Q models) or local site-effects (e.g., different high-frequency attenuation factor, k, for each recording station), as has been done in various studies, also for Greece [e.g., Margaris and Boore, 1998]. However, our target was to explore whether adequate fits can be obtained (for both macroseismic and seismic waveform data) by a handful of semi-automatically determined model parameters and not to obtain the optimal fit by modulating/optimizing several model parameters.

The obtained results suggest that in all cases we were able to reconstruct the main features of the damage pattern, as revealed by macroseismic data, as well as to also obtain an adequate simulation of the spectral content (FAS) of the available strong ground motion records. This good correlation was even more evident for the case of peak ground values (PGA and PGV), where the semi-automated, blind predictions, provided a satisfactory fit between observed and synthetic results. The joint evaluation of macroseismic and strong motion data helped to clarify discrepancies and bias observed for specific events (e.g., Alkyonides, 1981, **M**6.7 earthquake), where damage was amplified by the strong aftershock (**M**6.4) overprint on the mainshock impact.

The approach adopted in the present work can be further expended and improved. An important point concerns the quantitative assessment of site-effects on seismic motions. For example, while long-period effects due to near-field pulses are modeled in EXSIM by the analytical model of Mavroeidis and Papageorgiou [2003], deep basin long-period effects are only partly captured in the generic amplification functions shown in Fig. 5. There are several ways that this can be improved, e.g., by including in the simulation grid, areas with deep sediments for which 1D profiles are available [e.g. from actual geological-geophysical information or from V_{S30} to V_{SZ} proxies, e.g. Chiou and Youngs, 2008, 2014]. For these simulation points we could either adopt new (adapted) site amplification functions (based on the 1D profiles) that also model deep basin effects or use appropriate functional forms [e.g., Boore et al., 2014] to account for the deep basin effects on peak ground motions and spectral values. While this adapting is a demanding task, as it would require a grid of much more precise geological-geophysical information for all simulations, it is a feasible future improvement of the proposed approach.

Additional improvements can be also introduced in various other aspects of the modeling. For instance, the wave propagation path could be improved by using automatically generated local 1D velocity and Q models, extracted (averaged) from larger-scale 3D (e.g., tomographic) model. Moreover, an optimization of a minimal number of model parameters (e.g., of the stress parameter) could be used to obtain a zero-bias/smaller RMS misfit between observed and synthetic data. Furthermore, we could also benefit from detailed rupture models, since ground motions recorded at near-fault stations are strongly affected by local slip asperities along the fault. Of course, such optimizations cannot include too many model parameters, as this would make the problem rather non-unique or poorly constrained, unless a very large number of macroseismic and strong motion data is available. Therefore, similar optimizations need to be performed with caution, especially for older events for which limited information (often of poor accuracy) is available.

It should be noted that the previous conclusions are based on a rather small dataset (2437 Intensity Data Points from 4 events for the macroseismic data simulations and a small number of PGA and PGV information from 6 events, presented in Figure 19). This limitation is imposed by the fact that only for a handful of strong mainshocks, during a specific period (1978-1995) is an adequate number of data available. Despite this limitation, the qualitative and quantitative fits verify that the employed approach could be efficiently adopted for the simulation of macroseismic data from historical earthquakes, considering the intrinsic modeling limitations. Finally, the results suggest that a joint-misfit simultaneous simulation of macroseismic and strong motion data is a feasible target, that can be potentially employed for the simulation of older events, for which a limited number of instrumental data is often available [e.g. Zonno et al., 2010]. This approach would allow to use the lower accuracy but higher density macroseismic data to constrain the seismic source uncertainties provided by the limited strong motion datasets.

Data and resources. The EXSIM_DMB code used for the simulations is available at http://www.daveboore.com/software_online.html (last accessed December 2017). Macroseismic intensities of historical events were collected from the database of macroseismic information for the Aegean area [Papazachos et al., 1997]. Strong motion records were collected from the HEAD database (http://www.itsak.gr/head/) using data from the permanent strong-motion networks operated by the Institute of Engineering Seismology and Earthquake Engineering – ITSAK (http://www.itsak.gr/) and the Geodynamic Institute of the National Observatory of Athens (https://accelnet.gein.noa.gr/). Some plots were made using the Generic Mapping Tools software, version 5 [Wessel and Smith 1998; http://www.soest.hawaii.edu/gmt/, last accessed February 2019].

References

Abercrombie, R.E., I.G. Main, A. Douglas and P. Burton (1995). The nucleation and rupture process of the 1981 Gulf of Corinth earthquakes from deconvolved broad-band data, Geophys. J. Int., 120, 393-405. https://doi.org/10.1111/j.1365-246X. 1995.tb01827.x

Armijo, R., B. Meyer, G. C. P. King, A. Rigo, and D. Papanastassiou (1996). Quaternary Evolution of the Corinth Rift and Its Implications for the Late Cenozoic Evolution of the Aegean, Geophys. J. Int., 126, 11-53, https://doi.org/10.1111/j.1365-246X.1996.tb05264.x.

Atkinson, G. M., K. Assatourians, D. M. Boore, K. Campbell, and D. Motazedian (2009). A Guide to Differences between Stochastic Point-Source and Stochastic Finite-Fault Simulations, Bull. Seism. Soc. Am., 99, 3192-3201, https://doi.org/10.1785/0120090058.

Benetatos, C.A. and A.A. Kiratzi (2004). Stochastic Strong Ground Motion Simulation of Intermediate Depth Earthquakes: The Cases of the 30 May 1990 Vrancea (Romania) and of the 22 January 2002 Karpathos Island (Greece) Earthquakes, Soil Dyn. Earthq. Eng., 24, 1-9, https://doi.org/10.1016/j.soildyn.2003.10 .003.

Beresnev, I.A. and G.M. Atkinson (1999). Generic Finite-Fault Model for Ground-Motion Prediction in Eastern North America, Bull. Seism. Soc. Am., 89, 608-625.

Bernard, P., P. Briole, B. Meyer, H. Lyon-Caen, J.-M. Gomez, C. Tiberi, C. Berge, R. Cattin, D. Hatzfeld, C. Lachetl, B. Lebrun, A. Deschamps, F. Courboulex, C. Larroque, A. Rigo, D. Massonnet, P. Papadimitriou, J. Kassaras, D. Diagourtas, K. Makropoulos, G. Veis, E. Papazisi, C. Mitsakaki, V. Karakostas, E. Papadimitriou, D. Papanastasiou, M. Chouliaras and G. Stavrakakis (1997). The Ms = 6.2, June 15, 1995 Aigion Earthquake (Greece): Evidence for Low Angle Normal Faulting in the Corinth Rift, J. Seism., 1, 2, 131-150, https://doi.org/10.1023/A:1009795618839.

Boore, D.M. (1983). Stochastic Simulation of High-Frequency Ground Motions Based on Seismological Models of the Radiated Spectra, Bull. Seism. Soc. Am., 73, 1865-1894.

Boore, D.M. (2009). Comparing Stochastic Point-Source and Finite-Source Ground-Motion Simulations: SMSIM and EXSIM, Bull. Seism. Soc. Am., 99, 3202-3216, https://doi.org/10.1785/ 0120090056.

Boore, D.M. (2016). Determining Generic Velocity and Density Models for Crustal Amplification Calculations, with an Update of the Boore and Joyner (1977) Generic Site Amplification for Vs(Z)=760 m/s, Bull. Seism. Soc. Am., 106, 316-320, https://doi.org/ 10.1785/0120150229.

Boore, D.M. and G.M. Atkinson (1987). Stochastic Prediction of Ground Motion and Spectral Response Parameters at Hard-Rock Sites in Eastern North America. Bull. Seism. Soc. Am. 77, 440-467.

Boore, D.M. and W.B. Joyner (1997). Site Amplifications for Generic Rock Sites, Bull. Seism. Soc. Am., 87, 327-341.

Boore, D.M, J.P. Stewart, E. Seyhan, and G.M. Atkinson (2014). NGA-West2 equations for predicting PGA, PGV, and 5% damped PSA for shallow crustal earthquakes, Earthquake Spectra, 30, 3, 1057-1085.

Briole, P., A. Rigo, H. Lyon-Caen, J. C. Ruegg, K. Papazissi, C. Mitsakaki, A. Balodimou, G. Veis, D. Hatzfeld, and A. Deschamps (2000). Active Deformation of the Corinth Rift, Greece: Results from Repeated Global Positioning System Surveys between 1990 and 1995, J. Geophys. Res. Solid Earth, 105, 25605-25625, https://doi.org/10.1029/2000JB900148.

Chiou, B.J. and R.R. Youngs (2008). An NGA model for the average horizontal component of peak ground motion and response spectra, Earthquake spectra, 24, 1, 173-215.

Chiou, B.S.J. and R.R.Youngs (2014). Update of the Chiou and Youngs NGA model for the average horizontal component of peak ground motion and response spectra, Earthquake Spectra, 30, 3, 1117-1153.

Console R., R. Carluccio, E. Papadimitriou and V. Karakostas (2015). Synthetic Earthquake Catalogs Simulating Seismic Activity in the Corinth Gulf, Greece, Fault System, J. Geophys. Res. Solid Earth, 120, 320-343, https://doi.org/10.1002/2014JB011765.

Dang, P., and Q. Liu (2020). Stochastic Finite-Fault Ground Motion Simulation for the Mw 6.7 Earthquake in Lushan, China, Natural Hazards, 100, 3, 1215-1241, https://doi.org/10.1007/s11069-020-03859-3.

Ding, Y., G.P. Mavroeidis and N.P. Theodoulidis (2019). Simulation of Strong Ground Motion from the 1995 Mw 6.5 Kozani-Grevena, Greece, Earthquake Using a Hybrid Deterministic-Stochastic Approach, Soil Dyn. Earthq. Eng., 117, 357-373, https://doi.org/10.1016 /j.soildyn.2018.11.013.

Galluzzo, D., G. Zonno, and E. Del Pezzo (2008). Stochastic Finite-Fault Ground-Motion Simulation in a Wave-Field Diffusive Regime: Case Study of the Mt. Vesuvius Volcanic Area, Bull. Seism. Soc. Am., 98, 3, 1272-1288, https://doi.org/10.1785/0120070183.

Giannaraki, G., I. Kassaras, Z. Roumelioti, D. Kazantzidou-Firtinidou and A. Ganas (2019). Deterministic Seismic Risk Assessment in the City of Aigion (W. Corinth Gulf, Greece) and Juxtaposition with Real Damage Due to the 1995 Mw6.4 Earthquake, Bull. Earthq. Eng., 17 603-634, https://doi.org/10.1007/ s10518-018-0464-z.

Ghofrani, H., Atkinson, G.M., Goda, K. and Assatourians, K., (2013). Stochastic finite-fault simulations of the 2011 Tohoku, Japan, earthquake, Bull. Seism. Soc. Am., 103, 2B, 1307-1320.

Hatzidimitriou, P. M. (1993). Attenuation of coda waves in northern Greece, Pure Appl. Geophys., 140, 1, 63-78, https://doi.org/10.1007/BF00876871.

Hatzidimitriou, P. M. (1995). S-wave attenuation in the crust in northern Greece. Bull. Seism. Soc. Am., 85, 5, 1381-1387. https://doi.org/10.1785/BSSA0850051381.

Hatzfeld, D., V. Karakostas, M. Ziazia, G. Selvaggi, S. Leborgne, C. Berge, R. Guiguet, A. Paul, P. Voidomatis, D. Diagourtas, I. Kassaras, I. Koutsikos, K. Makropoulos, R. Azzara, M. Di Bona, S. Baccheschi, P. Bernard and Papaioannou, C. (1997). The Kozani-Grevena (Greece) Earthquake of 13 May 1995 Revisited from a Detailed Seismological Study, Seismol. Res. Lett., 6, 61-70.

Jackson, J.A., J. Gagnepain, G. Houseman, G.C.P. King, P. Papadimitriou, C. Soufleris and J. Virieux (1982). Seismicity, Normal Faulting, and the Geomorpho-logical Development of the Gulf of Corinth (Greece): The Corinth Earthquakes of February and March 1981, Earth Planet. Sc. Lett., 57, 377-397, https://doi.org/10.1016/0012-821X(82)90158-3.

Karakaisis, G.F., B.G. Karakostas, E.E. Papadimitriou, E.M. Scordilis and B.C. Papazachos (1985). Seismic Sequences in Greece Interpreted in Terms of Barrier Model, Nature, 315, 212-214, https://doi.org/10.1038/315212a0.

Kazantzidou-Firtinidou, D., I. Kassaras, A. Ganas, C. Tsimi, N. Sakellariou, S. Mourloukos, P. Stoumpos, K. Michalaki and G. Giannaraki (2016). Seismic damage scenarios in Kalamata (S. Greece), Bull. Geol. Soc. Gr., 50, 1495-1505, https://doi.org/10.12681/bgsg.11862.

Kiratzi, A.A. (1999). Stress Tensor Inversion in Western Greece Using Earthquake Focal Mechanisms from the Kozani-Grevena 1995 Seismic Sequence, Ann. Geophys., 42, 725-734. https://doi.org/10.4401/ag-3752.

Kkallas, Ch., C.B. Papazachos, D. Boore, Ch. Ventouzi and B.N. Margaris (2018). Historical Intermediate-Depth Earthquakes in the Southern Aegean Sea Benioff Zone: Modeling Their Anomalous Macroseismic Patterns with Stochastic Ground-Motion Simulations, Bull. Earthq. Eng., 16, 5121-5150, https://doi.org/ 10.1007/s10518-018-0342-8.

Klimis, N.S., B.N. Margaris and P.K. Koliopoulos (1999). Site-Dependent Amplification Functions and Response Spectra in Greece, J. Earthq. Eng., 3, 237-270, https://doi.org/10.1142/S1363246999000107.

Kramer, S.L. (1996). Geotechnical Earthquake Engineering, Prentice-Hall, N.J: Prentice Hall., 524, 3 Ann.

Lemoine, A., J. Douglas and F. Cotton (2012). Testing the Applicability of Correlations between Topographic Slope and VS30 for Europe, Bull. Seism. Soc. Am., 102, 2585-2299, https://doi.org/10.1785/0120110240.

Lyon-Caen, H., R. Armijo, J. Drakopoulos, J. Baskoutass, N. Delibassis, R. Gaulon, V. Kouskouna, J. Latoussakis, K. Makropoulos, P. Papadimitriou, D. Papanastassiou and G. Pedotti (1988). The 1986 Kalamata (South Peloponnesus) Earthquake: Detailed Study of a Normal Fault, Evidences for East-West Extension in the Hellenic Arc, J. Geophys. Res. Solid Earth, 93, 14967-15000, https://doi.org/10.1029/JB093iB12p14967.

Margaris, B.N and D.M. Boore (1998). Determination of Δσ and Ko from Response Spectra of Large Earthquakes in Greece, Bull. Seism. Soc. Am., 88, 170-182.

Margaris, B.N. and P.M. Hatzidimitriou (2002). Source Spectral Scaling and Stress Release Estimates Using Strong-Motion Records in Greece, Bull. Seism. Soc. Am., 92, 1040-1059, https://doi.org/10.1785/0120010126.

Mariolakos, I., D. Papanikolaou, N. Symeonidis, E. Lekkas, Z. Karotsieris, and C. Sideris (1982). The Deformation of the Area around the Eastern Korinth Gulf by the Earthquakes of February-March 1981, Proceedings, HEAT Symp., I, 400-420.

Mavroeidis, G.P. and A.S. Papageorgiou, A.S. (2003). A mathematical representation of near-fault ground motions, Bull. Seism. Soc. Am., 93, 3, 1099-1131.

Mavroeidis, G.P., Y. Ding, and N. Moharrami (2018). Revisiting the 1995 MW 6.4 Aigion, Greece, Earthquake: Simulation of Broadband Strong Ground Motion and Site Response Analysis, Soil Dyn. Earthq. Eng., 104, 156-173, https://doi.org/10.1016/j.soildyn. 2017.08.023.

Meyer, B., R. Armijo, D. Massonnet, J. B. de Chabalier, C. Delacourt, J. C. Ruegg, J. Achache, P. Briole and D. Papanastassiou (1996). The 1995 Grevena (Northern Greece) Earthquake: Fault Model Constrained with Tectonic Observations and SAR Interferometry, Geophys. Res. Lett., 23, 2677-2680, https://doi.org/ 10.1029/96GL02389.

Motazedian, D. and G.M. Atkinson (2005). Stochastic Finite-Fault Modeling Based on a Dynamic Corner Frequency, Bull. Seism. Soc. Am., 95, 995-1010, https://doi.org/10.1785/0120030207.

Motazedian, D. and Moinfar, A., (2006). Hybrid stochastic finite fault modeling of 2003, M6. 5, Bam earthquake (Iran), J. Seismol., 10, 1, 91-103.

Papanastassiou, D. (2002). Destructive Earthquakes and Seismotectonics in the Gulf of Corinth, Central Greece: A Review. In. In: Görür N., Papadopoulos G.A., Okay N. (eds) Integration of Earth Science Research on the Turkish and Greek 1999 Earthquakes. NATO Science Series: IV: Earth and Environmental Sciences, vol. 9. Springer, Dordrecht, https://doi.org/ 10.1007/978-94-010-0383-4_12

Papazachos, B., A. Kiratzi, B. Karakostas, D. Panagiotopoulos, E. Scordilis, and D. M. Mountrakis (1988). Surface Fault Traces, Fault Plane Solution and Spatial Distribution of the Aftershocks of the September 13, 1986 Earthquake of Kalamata (Southern Greece), Pure Appl. Geophys., 126, 55-68, https://doi.org/ 10.1007/BF00876914.

Papazachos, B.C. (1990). Seismicity of the Aegean and Surrounding Area, Tectonophysics, 178, 2-4, 287-308, https://doi.org/10.1016/0040-1951(90)90155-2.

Papazachos, B.C., D. Panagiotopoulos, E. Scordilis, G. Karakaisis, C. Papaioannou, B. Karakostas, E. Papadimitriou, A. Kiratzi, P. Hatzidimitriou, G. Leventakis, Ph. Voidomatis, K. Peftitselis, A. Savaidis and T. Tsapanos (1996). Focal Properties of the 13 May 1995 Large (Ms = 6.6) Earthquake in the Kozani Area (North Greece), Proceedings of the XV Congress of the Carpatho-Balcan Geological Assoc., Special Publication of The Geological Society of Greece, Athens Sept. 1995, 6: 99-106.

Papazachos, B.C., Ch. Papaioannou, C.B. Papazachos and A.S. Savvaidis (1997). Atlas of Isoseismal Maps for Strong Shallow Earthquakes in Greece and Surrounding Area (426BC-1995), Ziti publications, Thessaloniki, 176.

Papazachos, B.C., and C. Papazachou (1997). The Earthquakes of Greece, Ziti publications, Thessaloniki, 304.

Papazachos, B.C., E.M. Scordilis, D.G. Panagiotopoulos, C.B. Papazachos and G.F. Karakaisis (2004). Global relations between seismic fault parameters and moment magnitude of earthquakes, Bull. Geol. Soc. Gr., 36, 1482-1489, https://doi.org/10.12681/bgsg.16538.

Papazachos, C. and Ch. Papaioannou (1997). The macroseismic field of the Balkan Area, J. Seism., 1, 2, 181-201, https://doi.org/10.1023/A:1009709112995.

Papazachos, C. and G. Nolet (1997). P and S Deep Velocity Structure of the Hellenic Area Obtained by Robust Nonlinear Inversion of Travel Times, J. Geophys. Res. Solid Earth, 102, 8349-8367, https://doi.org/ 10.1029/96JB03730.

Papazachos, G., C. Papazachos, A. Skarlatoudis, H. Kkallas and E. Lekkas (2015). Modelling Macroseismic Observations for Historical Earthquakes: The Cases of the M = 7.0, 1954 Sofades and M = 6.8, 1957 Velestino Events (Central Greece), J. Seism., 20, 151-165, https://doi.org/10.1007/s10950-015-9517-9.

Ravnalis, M. (2020). Spatial distribution of damage from strong earthquakes in the Aegean area from the joint interpretation of macroseismic and instrumental data. MSc, Thesis Aristotle University of Thessaloniki, 184, 3 Annexes (in Greek).

Roumelioti, Z., A. Kiratzi, N. Theodulidis and C. Papaioannou (2000). A Comparative Study of a Stochastic and Deterministic Simulation of Strong Ground Motion Applied to the Kozani-Grevena (NW Greece) 1995 Sequence, Ann. Geophys., 43, 951-966, 10.4401/ag-3666.

Roumelioti, Z., A. Kiratzi and N. Theodoulidis (2004). Stochastic strong ground motion simulation of the 7 September 1999 Athens (Greece) earthquake, Bull. Seism. Soc. Am., 94, 3, 1036-1052. https://doi.org/10.1785/0120030219.

Roumelioti, Z., A., Kiratzi, B., Margaris, and A., Chatzipetros (2017). Simulation of strong ground motion on near-fault rock outcrop for engineering purposes: The case of the city of Xanthi (northern Greece), Bull. Earthq. Eng., 15, 1, 25-49. https://doi.org/10.1007/s10518-016-9949-9

Shebalin, N.V., V. Kárnik and D. Hadzievski (1974). Catalogue of Earthquakes 1901-1970, and Atlas of Isoseismal Maps. UNDP/UNESCO Balkan Project, Skopje 3.

Skarlatoudis, A.A., C.B. Papazachos and B.N. Margaris (2003). Determination of Noise Spectra from Strong Motion Data Recorded in Greece, J. Seism.7, 533-540, https://doi.org/10.1023/B:JOSE.0000005724.36224.58.

Stewart, J. P., N. Klimis, A. Savvaidis, N. Theodoulidis, E. Zargli, G. Athanasopoulos, P. Pelekis, G. Mylonakis and B. Margaris (2014). Compilation of a Local VS Profile Database and Its Application for Inference of VS30 from Geologic- and Terrain-Based Proxies, Bull. Seism. Soc. Am.,104 2827-2841.

Theodulidis, N., I. Kalogeras, C. Papazachos, V. Karastathis, B. Margaris, Ch. Papaioannou and A. Skarlatoudis (2004). HEAD 1.0: A Unified HEllenic Accelerogram Database, Seismol. Res. Lett., 75, 36-45, https://doi.org/10.1785/gssrl.75.1.36.

Trifunac, M.D. and M.I. Todorovska. (2001). A Note on the Useable Dynamic Range of Accelerographs Recording Translation, Soil Dyn. Earthq. Eng., 21 275-286, https://doi.org/10.1016/S0267-7261(01)00014-8.

Wald, D.J., V. Quitoriano, T.H. Heaton and H. Kanamori (1999). Relationships between Peak Ground Acceleration, Peak Ground Velocity, and Modified Mercalli Intensity in California, Earthquake Spectra, 15, 557-564, https://doi.org/10.1193/1.1586058.

Wald, D.J. and T.I. Allen (2007). Topographic slope as a proxy for seismic site-conditions (VS30) and amplification around the globe, Bull. Seism. Soc. Am., 97, 1379-1395.

Yolsal-Cevikbilen, S., and T. Taymaz (2012). Earthquake Source Parameters along the Hellenic Subduction Zone and Numerical Simulations of Historical Tsunamis in the Eastern Mediterranean, Tectonophysics, 536-537, 61-100, https://doi.org/ 10.1016/j.tecto.2012.02.019.

Zonno, G., C.S. Oliveira, M.A. Ferreira, G. Musacchio, F. Meroni, F. Mota-de-Sá, and F. Neves (2010). Assessing seismic damage through stochastic simulation of ground shaking: the case of the 1998 Faial Earthquake (Azores Islands), Surveys Geophys., 31, 3, 361-381, https://doi.org/10.1007/s10712-009-9091-1.

***CORRESPONDING AUTHOR: Michail RAVNALIS**,
Department of Geophysics, Aristotle University of Thessaloniki, Greece,
e-mail: mravnalis@gmail.com